Optica Applicata, Vol. XLVIII, No. 2, 2018
DOI: 10.5277/oa180207

Monte Carlo based angular analysis of multiple scattered photons for underwater optical imaging

SHENGFU LI*, RONGBO WANG, GUANGHUA CHEN

Institute of Fluid Physics, China Academy of Engineering Physics, Mianyang, 621900, China

*Corresponding author: lisfu2008@163.com

Image contrast and visibility associated with underwater optical imaging systems are usually degraded by the absorbing and scattering effects of turbid waters. To improve the image contrast, laser-range-gate has been widely applied to underwater optical imaging systems. The work of KATSEV *et al.* (Appl. Opt. 38(33), 1999, pp. 6849–6858) shows that the contrast of a shadow image is greater than that of the object image. The present paper outlines a Monte Carlo based simulation method of image formation for underwater optical imaging. It is found that the contrast of a shadow image varies with gate starting depths. The angular distribution of multiply scattered photons is obtained via semi-analytical models (SHENGFU LI *et al.*, Opt. Commun. 381, 2016, pp. 43–47). The simulated results show that increasing the gate starting depth can reduce the highly backscattered photons, thus can improve the image contrast.

Keywords: underwater imaging, turbid media, Monte Carlo method, multiple scattering.

1. Introduction

Underwater optical imaging (UOI) has been of long-standing interest to researchers due to its great importance in military and civilian applications [3]. Image contrast and visibility associated with UOI systems are usually degraded by the absorbing and scattering effects of turbid waters. To improve the image quality, laser-range-gate (LRG) has been applied to UOI systems due to its ability to effectively eliminate the influence of backscatter and its associated noise [4–12].

Figure 1 illustrates the principle of laser-range-gate underwater optical imaging (LRGUOI) system. Briefly, the light source emits a short illumination pulse (<10 ns) and the receiver is kept closed until time $t_0 = 2d/c$, and then opened for a short time $\Delta t = 2\Delta d/c$ (here c is the light speed in water medium, d is the distance from the receiver to the object, Δd is the desired depth of view) as shown in Fig. 1. This LRG scheme recovers the object image by using the reflective character of the object. KATSEV *et al.* theoretically investigated another LRG scheme which utilizes the transmittance of

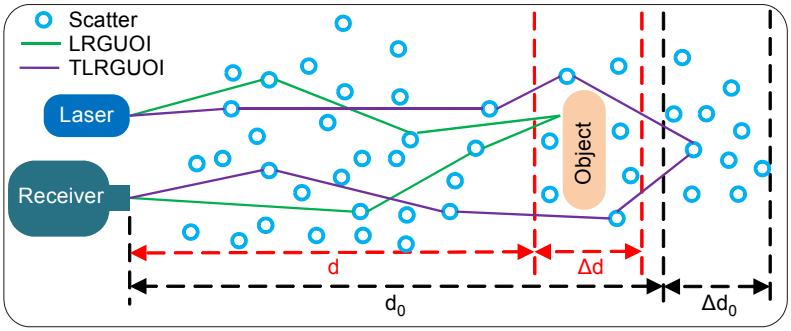

Fig. 1. Schematic of LRGUOI and TLRGUOI. d (d_0) and Δd (Δd_0) are the parameters of LRGUOI (TLRGUOI). The green (purple) lines show the photon path for LRGUOI (TLRGUOI).

objects [1], hereafter called the TLRGUOI: the receiver is kept closed until time $t_0 = 2d_0/c$, and then opened for a short time $\Delta t = 2\Delta d_0/c$ (here d_0 is larger than the distance from the receiver to the object) as shown in Fig. 1. While the imaging scheme using transmittance has been widely analyzed in inline holograph [13–15] and shadowgraph [16, 17], all of these works targeted on the scene that the object (particles) are embedded into a transparent medium and thus are different from TLRGUOI. KATSEV *et al.* investigated the image contrast by using an analytical model and found that the contrast of a shadow image was greater than that of the object image and varied with gate starting depths [1]. However, they did not offer explanations for this point, probably because the analytical model cannot be used to analyze the behavior of multiple scattered photons.

This paper outlines a Monte Carlo based simulation method of image formation for underwater optical imaging, and analyzes the behavior of multiple scattered photons from different perspectives. While Monte Carlo models have been used in a variety of simulations [18–22] due to their generality and being easy-to-implementation, all of these studies target on the optical fluence and cannot be directly extended on the present problem.

Our Monte Carlo based simulation model for TLRGUOI is described in Sections 2 and 3. Based on the simulation model, we have analyzed the angular distribution of multiple scattered photons as our recent work [2], we also investigated the effects of different scattering orders on the optical fluence. The simulated results and associated discussions are given in Section 4.

2. Simulation configuration

For the sake of convenience, we consider a cylindrically symmetric scene, as shown in Fig. 2. A cylindrical object with a radius of r_0 and a height of h is embedded into a homogenous medium (water medium). A Cartesian coordinate system is defined; the z-axis is parallel to the axis of the cylindrical object. Suppose that the initial positions

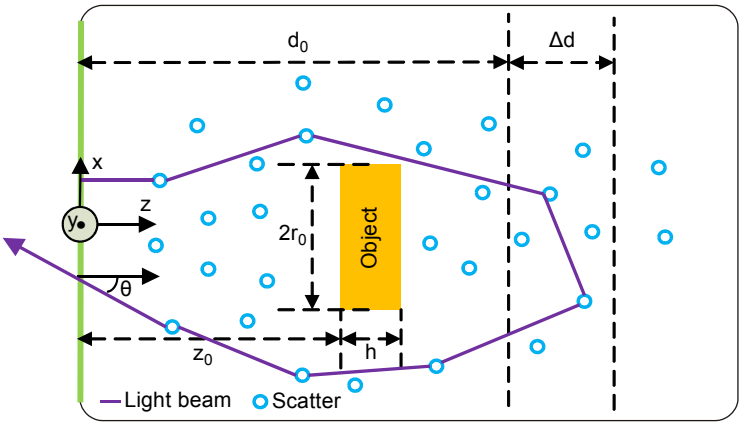

Fig. 2. Schematic of the configuration of MC simulation.

of photons in MC simulations are distributed on the *xy*-plane (green line), our task is to record the photon fluence $I_\theta^l(x, y, z, S)$, here l is a positive integer and represents the scattering order, θ is defined with respect to the z-axis, S represents the photon's path length, as the purple line in Fig. 2.

3. Simulation model

3.1. Simulation flowchart

Our MC simulation model adopted a standard MC model as in [18]. Briefly, this standard MC model consists of the following steps:

Step 1. It launches a photon;

Step 2. It stochastically determines the scattering direction and path length of the photon to calculate the new location of the photon after a scattering event;

Step 3. It reduces the photon energy;

Step 4. It repeats steps 2 and 3 until the photon energy is less than a threshold (the photon is dead, $P_{\text{state}} = 0$, see Fig. 3); and

Step 5. It repeats steps 1–4 until the number of photons meets the required precision.

More detailed information can be found in associated references [18–22], and the black parts in Fig. 3. Step 2 derives the scattering direction from Henyey–Greenstein phase function. To implement a simulation with MC, three parameters are required: the absorption coefficient μ_a, the scattering coefficient μ_s, and the anisotropy factor g.

3.2. Send a photon

Suppose that our MC model deals with the transport of a circularly flat beam with a radius of R, the initial position of a photon can be assigned as $(\xi R, 0, 0)$. Here, ξ is a random number and uniformly distributed over the interval (0, 1). As in [2], the initial direction

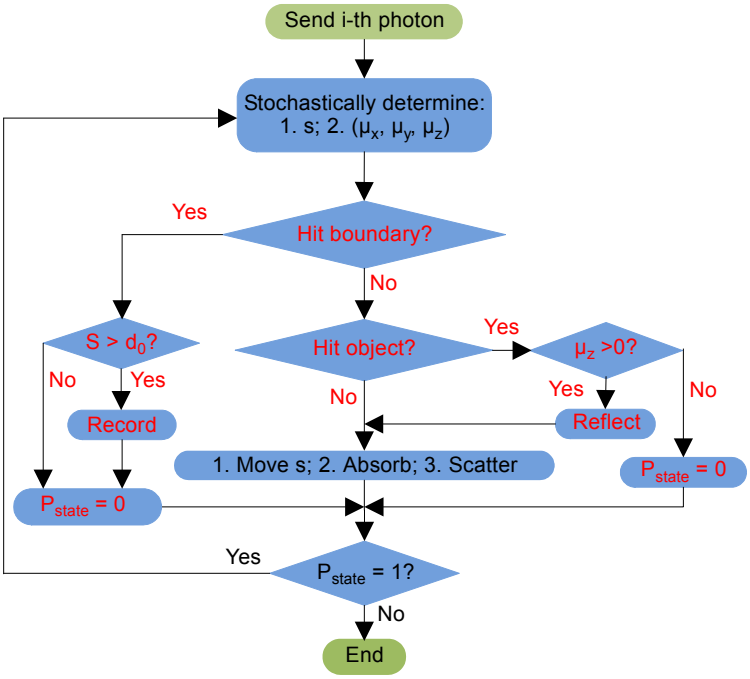

Fig. 3. Flowchart of our simulation. Black parts represent conventional MC flowchart. Red parts are our contributions. S – total path length, and s – path length in each step.

of a photon is specified by the directional cosines (μ_x, μ_y, μ_z). For our simulation configuration, the initial direction is assigned as (0, 0, 1).

3.3. Object simulation

Considering that TLRGUOI utilizes the transmittance of objects, we simulate an object with an infinitely thin (h in Fig. 2 approaches 0) cylinder and suppose that the object is opaque.

During a step s, a photon packet may hit the object. Let (x, y, z) denote the current position of the photon and let (μ_x, μ_y, μ_z) be the current direction, then if s and (μ_x, μ_y, μ_z) meet the following formula, the photon is to hit the object,

$$\begin{cases} s > (z_o - z)/\mu_z \\ r_0 > \sqrt{x_1^2 + y_1^2} \end{cases} \tag{1}$$

here,

$$\begin{cases} x_1 = x + (z - z_o)\mu_x/\mu_z \\ y_1 = y + (z - z_o)\mu_y/\mu_z \end{cases} \tag{2}$$

and z_o is the depth of the object. In such situations, if $\mu_z > 0$, it is processed as reflection. If $\mu_z < 0$, it is terminated since $\mu_z < 0$ indicates $z > z_o$ and thus it has a small probability to return to the *xy*-plane in Fig. 2.

3.4. Recording data

During the simulation, the photon fluence $I(x, y, z)$ is recorded and can be expressed as,

$$I(x, y, z) = \sum_l \int_{-\pi/2}^{\pi/2} \mathrm{d}\theta \int_S I_\theta^l(x, y, z, S)\,\mathrm{d}S \tag{3}$$

The image quality is determined by $I(x, y, z = 0)$. For TLRGUOI, $I(x, y, z = 0)$ can be written as,

$$I(x, y, z = 0) = \sum_l \int_{-\pi/2}^{\pi/2} \mathrm{d}\theta \int_{d_0}^{d_0 + \Delta d} I_\theta^l(x, y, z = 0, S)\,\mathrm{d}S \tag{4}$$

The angular analysis of the contribution of multiple scattered photons to the image contrast is to be implemented via,

$$A(\theta) = \sum_l \int_\Omega \mathrm{d}x\mathrm{d}y \int_{d_0}^{d_0 + \Delta d} I_\theta^l(x, y, z = 0, S)\,\mathrm{d}S \tag{5}$$

and the effect of different scattering orders on the image contrast is investigated by

$$SC(l) = \int_{-\pi/2}^{\pi/2} \mathrm{d}\theta \int_\Omega \mathrm{d}x\mathrm{d}y \int_{d_0}^{d_0 + \Delta d} I_\theta^l(x, y, z = 0, S)\,\mathrm{d}S \tag{6}$$

where θ can be obtained by $\theta = a\cos(-\mu_z)$, and Ω represents the *xy*-plane.

4. Simulation tests and results

In this section, several simulation examples are provided to show the feasibility of the proposed simulation method. All of the following simulations are based on the geometry shown in Fig. 2.

4.1. Validation

This section first tests our program with the following optical properties: $\mu_a = 0.2\ \mathrm{m}^{-1}$, $\mu_s = 0.2\ \mathrm{m}^{-1}$, $g = 1$, $z_o = 3$ m, $r_0 = 3$ m, $d_0 = 5$ m and $\Delta d = 10$ m. According to the physical meaning of g [18], when $g = 1$, all photons keep the initial direction (except the photons that hit the object) and thus there are no photons to undergo a path length ranging from $2d_0$ to $2(d_0 + \Delta d)$ and hit the green line in the geometry shown in Fig. 2.

Figure 4 shows the optical fluence distribution in medium and is in good agreement with the physical meaning: the incident photons keep the initial direction (0, 0, 1) and

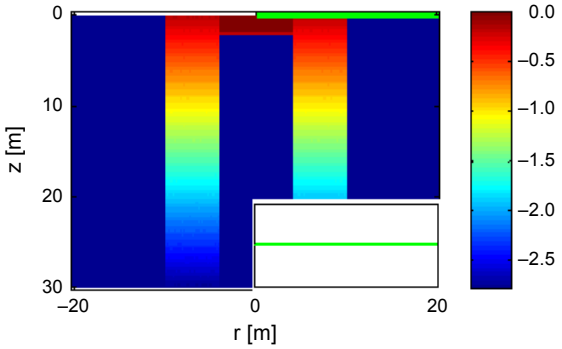

Fig. 4. Photon fluence distribution obtained by Eq. (3) for the following optical properties: $\mu_a = 0.2$ m^{-1}, $\mu_s = 0.2$ m^{-1}, $g = 1$, $r_0 = 3$ m, $z_o = 3$ m, $d_0 = 5$ m and $\Delta d = 10$ m. The inset shows the photon fluence distribution along the green line in the simulation configuration (see also Fig. 2) obtained by Eq. (4).

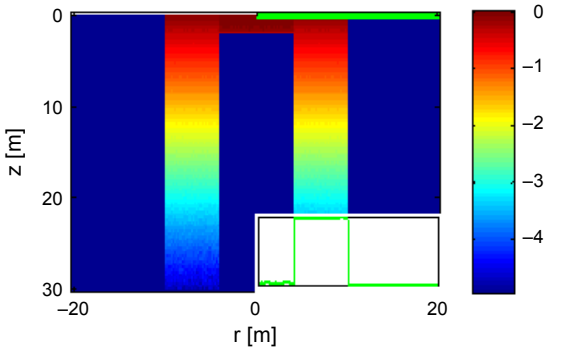

Fig. 5. Photon fluence distribution obtained by Eq. (3) for the following optical properties: $\mu_a = 0.2$ m^{-1}, $\mu_s = 0.2$ m^{-1}, $g = -1$, $r_0 = 3$ m, $z_o = 3$ m, $d_0 = 5$ m and $\Delta d = 10$ m. The inset shows the photon fluence distribution along the green line in the simulation configuration (see also Fig. 2) obtained by Eq. (4).

do not deviate into other directions. Note that the optical fluence distribution was normalized by its maximum value and is shown in log-scale. The inset shows the recorded photon fluence obtained by Eq. (4). The recorded photon fluence is zero and further confirms the feasibility of the proposed simulation method. Since our geometry is cylindrically symmetric, we chose to record the associated physical quantity as a function of (r, z), here $r = (x^2 + y^2)^{1/2}$ and the definition of (x, y, z) has been given before.

Our program was also validated with the special case $g = -1$ and other parameters were the same as the previous simulation. Figure 5 shows the optical fluence distribution and the photon fluence distribution obtained by Eq. (4). Figure 5 is in good agreement with the physical meaning of $g = -1$ ($g \to -1$ gives highly peaked backward scattering). The object boundary can be clearly found in Fig. 5. The inset shows the recorded photon fluence over the interval (0 m, 3 m) is not equal to 0. This arises from the reflectance from the object.

4.2. TLRGUOI simulation with typical parameters

Figures 4 and 5 show that the proposed simulation method can be used to simulate TLRGUOI. This section applies this method to the cases with typical optical properties: $\mu_a = 0.2\ m^{-1}$, $\mu_s = 0.2\ m^{-1}$, and $g = 0.9$. Other parameters were the same as the previous simulation.

Figure 6 shows the optical fluence distribution. In this case, the incident photons deviate from the initial direction into other directions. This is in good agreement with the physical meaning of $g = 0.9$ (it is not equal to 1 or –1).

As illustrated before, there are two key parameters for a TLRGUOI system: d_0 and Δd. In this section, we finished TLRGUOI simulations for various Δd while keeping d_0 fixed to 5 m. Figure 7 shows the corresponding photon fluence obtained by Eq. (3). The curves in Fig. 7 show that increasing Δd cannot help to improve the image quality.

We also finished TLRGUOI simulations for various d_0 while keeping Δd fixed to 10 m. Figure 8 shows the photon fluence obtained by Eq. (3). The curves in Fig. 8 show that increasing d_0 can help to improve the image quality: the photon fluence over the in-

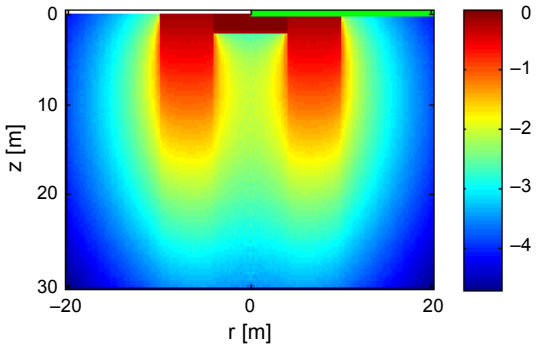

Fig. 6. Optical fluence distribution obtained by our simulation method for the following optical properties: $\mu_a = 0.2\ m^{-1}$, $\mu_s = 0.2\ m^{-1}$, $g = 0.9$ and $z_o = 3$ m.

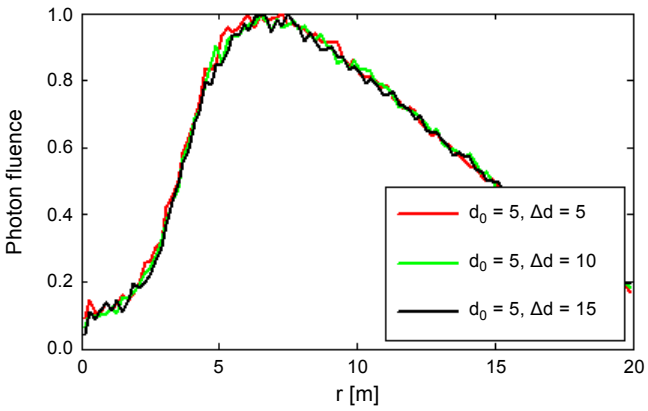

Fig. 7. Optical fluence obtained by Eq. (4) for various Δd while keeping d_0 fixed.

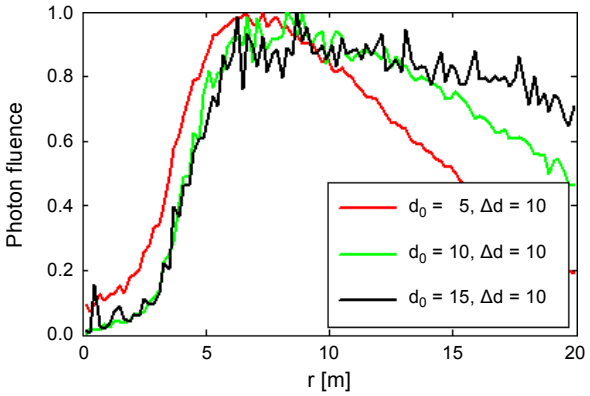

Fig. 8. Photon fluence obtained by Eq. (4) for various d_0 while keeping Δd fixed.

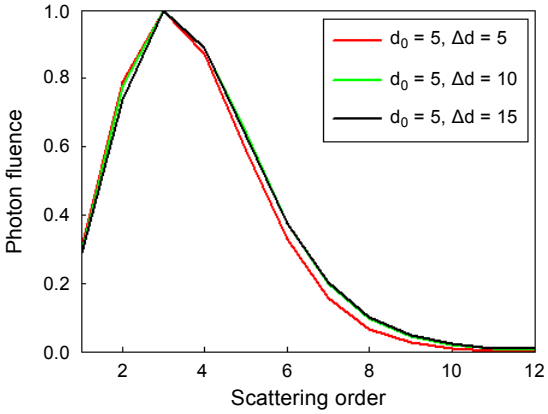

Fig. 9. Contribution of different scattering orders to the image $I(x, y, z = 0)$ for the parameters corresponding to Fig. 7.

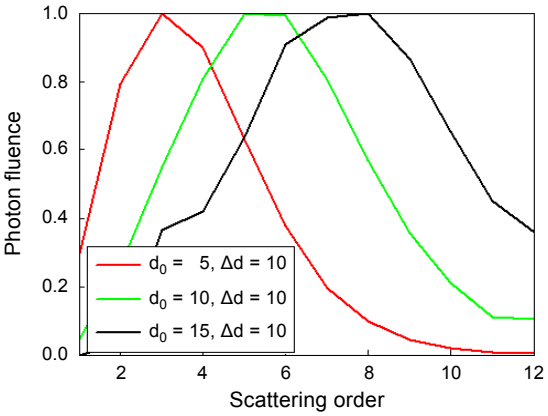

Fig. 10. Contribution of different scattering orders to the image $I(x, y, z = 0)$ for the parameters corresponding to Fig. 8.

terval (0 m, 3 m) approaches 0 as d_0 increases. Meanwhile, increasing d_0 reduces the number of photons that return to the xy-plane. This indicates that an optimal d_0 exists.

Figures 9 and 10 plot the contribution of different scattering orders to the image $I(x, y, z = 0)$ for the situations corresponding to Figs. 7 and 8, respectively. These curves were obtained by using Eq. (6). It can be seen that the curves in Fig. 9 are of the same shape. By contrast, increasing d_0 shifts the peak of the curves to larger scattering orders, as shown in Fig. 10. This indicates that the difference of the image contrast in Figs. 7 and 8 arises from multiple scattered photons.

Figures 11 and 12 plot the angular distribution obtained by Eq. (5) for the situations corresponding to Figs. 7 and 8, respectively. It can be seen from Fig. 12 that increasing d_0 can reduce the influence of the highly backscattered photons (the photons with large θ, see Fig. 2) on the image contrast, and thus optimizes the image contrast. The in-

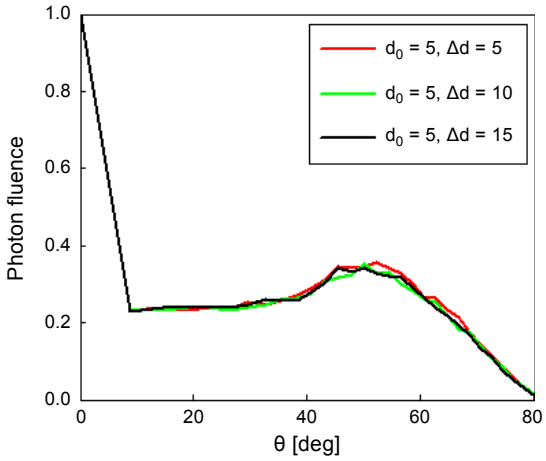

Fig. 11. Angular distribution obtained by Eq. (5) for the parameters corresponding to Fig. 7.

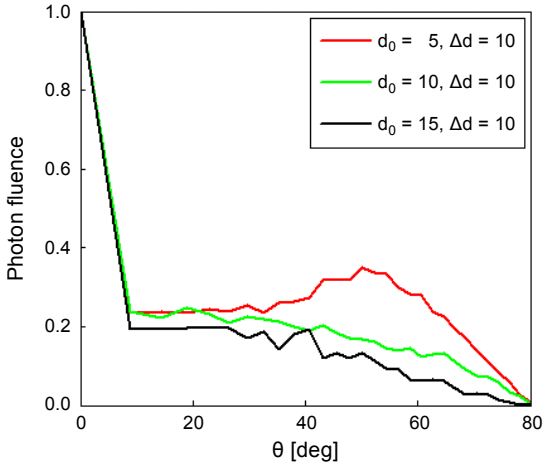

Fig. 12. Angular distribution obtained by Eq. (5) for the parameters corresponding to Fig. 8.

fluence of the highly scattered photons falls sharply when d_0 goes from 5 to 10 m, and it falls more slightly when d_0 goes from 15 to 20 m. By contrast, the angular distribution stays constant for various Δd, thus increasing Δd cannot help to improve the image contrast, as shown in Fig. 7. It is important to keep in mind that the increase in d_0 improves the object's image contrast, but leads to a decrease in energy.

In the present paper, the object in Fig. 2 is replaced with an infinitely thin cylinder. Although the real objects can never be infinitely thin, it can be so treated if the main task is to simulate the transmittance of objects, as TLRGUOI. However, it is straightforward to extend the proposed simulation method to objects of finite size. The proposed method can also be used to simulate conventional LRGUOI.

The red curve in Fig. 8 is smoother than the other curves. This is due to the fact that the number of photons decreases as d_0 increases. The authors believe that one can obtain smoother versions by increasing the number of incident photons. Figure 8 also shows an optimized d_0 exists for our geometry. If it is too large, the accumulated photon energy will be very small. Meanwhile, larger d_0 produces better image quality. Therefore, one should choose appropriate parameters for TLRGUOI, especially d_0.

There is one point the authors would like to stress. Indeed, increasing Δd cannot help to improve the image contrast. However, if it is too small, the accumulated photon energy will be very small. Practically, one should choose Δd based on the accumulated photon energy required by the receiver.

5. Conclusions

In this paper, we outlined a Monte Carlo based simulation model for LRGUOI. This simulation method was first validated with special cases, and then applied to the cases with typical optical properties. Using this simulation model, we numerically analyzed the angular distribution of multiple scattered photons and also investigated the effects of different scattering orders on the image contrast. Simulation results prove the feasibility of the proposed simulation model and show that the increase in d_0 reduces the influence of the highly scattered photons and thus improves the image contrast.

Acknowledgments – This study was financially supported by Science Challenge Project (TZ2016001), and National Natural Science Fund of China (11702275, 11672275).

References

[1] KATSEV I.L., ZEGE E.P., PRIKHACH A.S., *Image formation with regard to object shadow for objects inside a scattering medium*, Applied Optics 38(33), 1999, pp. 6849–6858.

[2] SHENGFU LI, GUANGHUA CHEN, RONGBO WANG, ZHENGXIONG LUO, QIXIAN PENG, *Monte Carlo based angular distribution estimation method of multiply scattered photons for underwater imaging*, Optics Communications 381, 2016, pp. 43–47.

[3] YUZHANG CHEN, WEI LI, MIN XIA, QING LI, KECHENG YANG, *Super-resolution reconstruction for underwater imaging*, Optica Applicata **41**(4), 2011, pp. 841–853.

[4] YOUWEI HUANG, FENGMEI CAO, WEIQI JIN, SU QIU, *Underwater pulsed laser range-gated imaging model and its effect on image degradation and restoration*, Optical Engineering 53(6), 2013, article ID 061608.

[5] CHING TAN, SLUZEK A., SEET G., *Model of gated imaging in turbid media*, Optical Engineering 44(11), 2005, article ID 116002.
[6] GUAN JIN-GE, ZHU JING-PING, TIAN HENG, *Polarimetric laser range-gated underwater imaging*, Chinese Physics Letters **32**(7), 2015, article ID 074201.
[7] XIA WANG, LING HU, QIANG ZHI, ZHEN-YUE CHEN, WEI-QI JIN, *Influence of range-gated intensifiers on underwater imaging system SNR*, Proceedings of SPIE 8912, 2013, article ID 89120E.
[8] HECKMAN P., HODGSON R., *Underwater optical range gating*, IEEE Journal of Quantum Electronics 3(11), 1967, pp. 445–448.
[9] JAFFE J.S., *Computer modeling and the design of optimal underwater imaging systems*, IEEE Journal of Oceanic Engineering 15(2), 1990, pp. 101–111.
[10] STRAND M.P., *Imaging model of underwater range-gated imaging systems*, Proceedings of SPIE 1537, 1991, pp. 151–160.
[11] SWARTZ B.A., *Laser range gate underwater imaging advances*, [In] *Proceedings OCEANS'94. Oceans Engineering for Today's Technology and Tomorrow's Preservation*, Vol. 2, IEEE, Brest, France, 1994, pp. II-722–II727.
[12] MCLEAN E.A., BURRIS H.R., STRAND M.P., *Short-pulse range-gated optical imaging in turbid water*, Applied Optics 34(21), 1995, pp. 4343–4351.
[13] BRADY D.J., CHOI K., MARKS D.L., HORISAKI R., LIM S., *Compressive holography*, Optics Express 17(15), 2009, pp. 13040–13049.
[14] DENIS L., LORENZ D., THIÉBAUT E., FOURNIER C., TREDE D., *Inline hologram reconstruction with sparsity constraints*, Optics Letters 34(22), 2009, pp. 3475–3477.
[15] RIVENSON Y., STERN A., ROSEN J., *Reconstruction guarantees for compressive tomographic holography*, Optics Letters 38(14), 2013, pp. 2509–2511.
[16] VAN HULSTEYN D.B., BENJAMIN R.F., *X-ray shadowgraphing in laser-produced plasma experiments*, Optics Letters 1(2), 1977, pp. 76–78.
[17] WOOD C.F., LEACH D.H., JIAN-ZHI ZHANG, CHANG R.K., BARBER P.W., *Time-resolved shadowgraphs of large individual water and ethanol droplets vaporized by a pulsed CO_2 laser*, Applied Optics 27(11), 1988, pp. 2279–2286.
[18] WANG L., JACQUES S.L., *Monte Carlo Modeling of Light Transport in Multi-layered Tissues in Standard C*, University of Texas M. D. Anderson Cancer Center, 1992.
[19] QIANQIAN FANG, BOAS D.A., *Monte Carlo simulation of photon migration in 3D turbid media accelerated by graphics processing units*, Optics Express 17(22), 2009, pp. 20178–20190.
[20] LIHONG WANG, JACQUES S.L., LIQIONG ZHENG, *MCML – Monte Carlo modeling of light transport in multilayered tissues*, Computer Methods and Programs in Biomedicine 47(2), 1995, pp. 131–146.
[21] WILSON B.C., ADAM G., *A Monte Carlo model for the absorption and flux distributions of light in tissue*, Medical Physics 10(6), 1983, pp. 824–830.
[22] MROCZKA J., SZCZEPANOWSKI R., *Modeling of light transmittance measurement in a finite layer of whole blood – a collimated transmittance problem in Monte Carlo simulation and diffusion model*, Optica Applicata **35**(2), 2005, pp. 311–331.

Received July 8, 2017
in revised form September 23, 2017